Biomedical Physics &
Engineering Express

Endorsed by IPEM Institute of Physics and Engineering in Medicine
PURPOSE-LED PUBLISHING™

PAPER

Permeation dynamics of organic moiety-tuned organosilica nanoparticles across porcine corneal barriers: experimental and mass transfer analysis for glaucoma drug delivery

To cite this article: Yifan Sun *et al* 2025 *Biomed. Phys. Eng. Express* **11** 045015

Biomedical Physics & Engineering Express

PAPER

Permeation dynamics of organic moiety-tuned organosilica nanoparticles across porcine corneal barriers: experimental and mass transfer analysis for glaucoma drug delivery

RECEIVED
20 February 2025

REVISED
27 May 2025

ACCEPTED FOR PUBLICATION
4 June 2025

PUBLISHED
17 June 2025

Yifan Sun[1,2,5], **Hengjun Mei**[2,5], **Hongguang Cui**[2], **Maomao Song**[3], **Yonghui Qiao**[1,*], **Jian Chen**[4,*] **and Yuan Lei**[3,*]

[1] School of Power and Energy, Northwestern Polytechnical University, Shaanxi, 710129, People's Republic of China
[2] The First Affiliated Hospital, Zhejiang University School of Medicine, Hangzhou, 310003, People's Republic of China
[3] Department of Ophthalmology & Visual Science, Eye & ENT Hospital, Shanghai Medical College, Fudan University, Shanghai, 200031, People's Republic of China
[4] School of Energy and Power Engineering, University of Shanghai for Science and Technology, Shanghai, 200093, People's Republic of China
[5] Yifan Sun and Hengjun Mei contributed equally to this paper.
[*] Authors to whom any correspondence should be addressed.

E-mail: yhqiao@nwpu.edu.cn (**Y Qiao**), 09900589r@connect.polyu.hk (**J Chen**) **and** yuan_lei@fudan.edu.cn (**Y Lei**)

Keywords: transcorneal permeation, hollow mesoporous organosilica, nanoparticles, glaucoma, porcine eye

Abstract

Elevated intraocular pressure is a key pathogenic factor in glaucoma, often leading to irreversible vision loss. In previous studies, we developed a novel hollow mesoporous organosilica nanocarrier functionalized with manganese(III) tetrakis(1-methyl-4-pyridyl)porphyrin (HMMN), demonstrating superior efficacy in treating primary open-angle glaucoma. This study presents a comparative analysis of the transcorneal permeability of HMMNs modified with thioether, biphenyl, and thioether/phenylene moieties in the porcine eye. Transcorneal permeability was evaluated using fluorescence intensity measurements in the porcine aqueous humor, followed by the calculation of diffusion and apparent permeability coefficients (Papp). Results reveal that thioether-modified HMMN exhibits significantly enhanced corneal permeability compared to biphenyl and thioether/phenylene-modified variants, with a diffusion coefficient of 4.88×10^{-6} $cm^2 s^{-1}$ and a Papp of 1.30×10^{-5} $cm\ s^{-1}$ in the porcine eye. These findings provide valuable insights into the permeability properties of hollow mesoporous organosilica nanocarriers, positioning them for broader applications in the treatment of various ocular diseases and potentially beyond. Furthermore, this work serves as a valuable reference for future studies exploring the potential of hybridized hollow mesoporous organosilica nanoparticles functionalized with diverse organic moieties for enhanced therapeutic outcomes.

1. Introduction

Glaucoma is caused by optic nerve damage and loss of retinal ganglion cells, typically associated with increased intraocular pressure (IOP) [1]. The increase in IOP may be the closure of the anterior chamber angle due to the forward movement of the lens along the axial direction of the eye, which obstructs the flow of aqueous humor from the posterior chamber through the pupil into the anterior chamber [2]. This type of glaucoma is called primary angle-closure glaucoma (PACG). Laser peripheral iridectomy is a common and effective treatment for PACG [3]. Another type of glaucoma is primary open-angle glaucoma (POAG). The cause of elevated IOP in this type of glaucoma is the increased resistance to aqueous humor outflow at the trabecular meshwork (TM) and Schlemm's canal (SC) [4]. The treatment for PACG mainly focuses on reducing the resistance at the TM and SC, such as selective laser trabeculoplasty [5], femtosecond laser trabeculotomy [4], and topical drug therapy. Among various therapeutic approaches, topical drug therapies remain the primary treatment modality [6]. However, topical drug therapies remain challenging due to the limitation of conventional drug delivery methods, such as topical administration via eye drops or ointments [7].

Table 1. Formulation Components of HMMN with Different Organic Moieties.

Formulations	Silica precursor	Organic moiety
HMMN1 (Thioether-Modified)	BTES (bis[3(triethoxysilyl)propyl]tetrasulfide); TEOS (tetraethyl orthosilicate)	MnTMPyP
HMMN2 (Biphenyl-Modified)	BTEBP (1,4-bis(triethoxysilyl)biphenyl); TEOS	MnTMPyP
HMMN3 (Thioether/Phenylene-Modified)	BTEB (1,4-bis(triethoxysilyl)benzene); BTES; TEOS	MnTMPyP

These traditional approaches face significant obstacles, including the physiological barriers of the cornea, conjunctiva, and tear film, resulting in low bioavailability of the administered drugs [8]. To maintain therapeutic drug levels, frequent dosing is often required, which can lead to toxicity [7] and reduce patient compliance [9].

To address these issues, various nanocarriers have been developed, including liposomes [10], micelles [11], nanoparticles [12], dendrimers [13] and hydrogels [14]. These nanocarriers have shown promise in enhancing drug delivery for ocular diseases, including glaucoma [15, 16]. Nitric oxide (NO) is a known regulator of the aqueous humor outflow pathway [17, 18], but its endogenous production is impaired in patients with primary open-angle glaucoma [19]. Exogenous NO supplementation, therefore, becomes necessary, but its delivery to target tissues is hampered by poor corneal penetration. Moreover, excess NO can react with endogenous superoxide anions to produce peroxynitrite, which disrupts anterior segment tissues, potentially leading to increased intraocular pressure [20]

To overcome these challenges, a novel nanocarrier, hollow mesoporous organosilica with MnTMPyP (manganese(III) tetrakis(1-methyl-4-pyridyl)porphyrin) nanoparticle (HMMN), was developed in our previous work [21]. Featuring high surface area, uniform mesopores, and various framework compositions, hollow mesoporous organosilica particles present broad and promising applications in tumor therapy [22, 23], bioimaging [24, 25], and ocular drug delivery [26, 27]. The HMMN not only enhances corneal permeability but also scavenges peroxynitrite, reducing its detrimental effects. Despite its potential, previous studies primarily relied on fluorescence imaging to assess the corneal penetration of different organic moiety-modified nanocarriers, lacking comprehensive quantitative data.

The application of mass transfer principles has significantly contributed to the study of drug transport in biological systems. Natesan *et al* employed a Franz diffusion cell to evaluate the permeation of resveratrol and quercetin co-encapsulated in chitosan nanoparticles, demonstrating that these nano-formulations significantly enhanced transcorneal permeation compared to free drugs [28]. Other studies have similarly demonstrated the enhanced permeability of nanocarrier-based formulations compared to traditional methods [29, 30]. However, the Franz diffusion cell presents limitations, such as poor simulation of the physiological corneal curvature, potential stromal swelling, and the inability to supply nutrients to corneal cells, which can affect nanocarrier penetration [31, 32]. To address these issues, a whole-eye model was employed in this study to investigate the transcorneal diffusion characteristics of HMMN.

This study systematically examines the corneal permeability of HMMN modified with different organic moieties by conducting permeation experiments and calculation of diffusion and apparent permeability coefficients. This work serves as a valuable reference for future studies exploring the potential of hybridized hollow mesoporous organosilica nanoparticles functionalized with various organic moieties for enhanced therapeutic applications.

2. Materials and methods

2.1. Materials

Three distinct nanocarriers were synthesized by co-hybridizing MnTMPyP with three different organic moieties: thioether, biphenyl, and thioether/phenylene. For ease of description, the nanocarriers modified with thioether, biphenyl, and thioether/phenylene are designated as HMMN1, HMMN2, and HMMN3, respectively. The Formulation Components of HMMN1/2/3 was depicted in table 1. The size of nanocarriers is in the range of 40–50 nm. Each nanocarrier was subsequently modified with fluorescein isothiocyanate (FITC) to produce solutions at a concentration of 15 mg mL^{-1} in phosphate buffer solutions (PBS) with PH 7.4. The study utilized 105 porcine eyeballs, and fluorescence measurements were conducted using a SpectraMax i3x microplate reader (Molecular Devices, San Jose, CA, USA) in conjunction with black 96-well plates (JingAn Biological, Shanghai, China). This study adhered to the principles of the Declaration of Helsinki and complied with all relevant medical ethical standards.

2.2. Methods

2.2.1. Permeation experiments

The permeation experiments were conducted using a specially designed setup (figure 1). To prevent the fluorescence of FITC under light exposure, the entire donor chamber was wrapped in tin foil, which also helped minimize the evaporation of the solution inside the chamber. Porcine eyes were placed in the pits

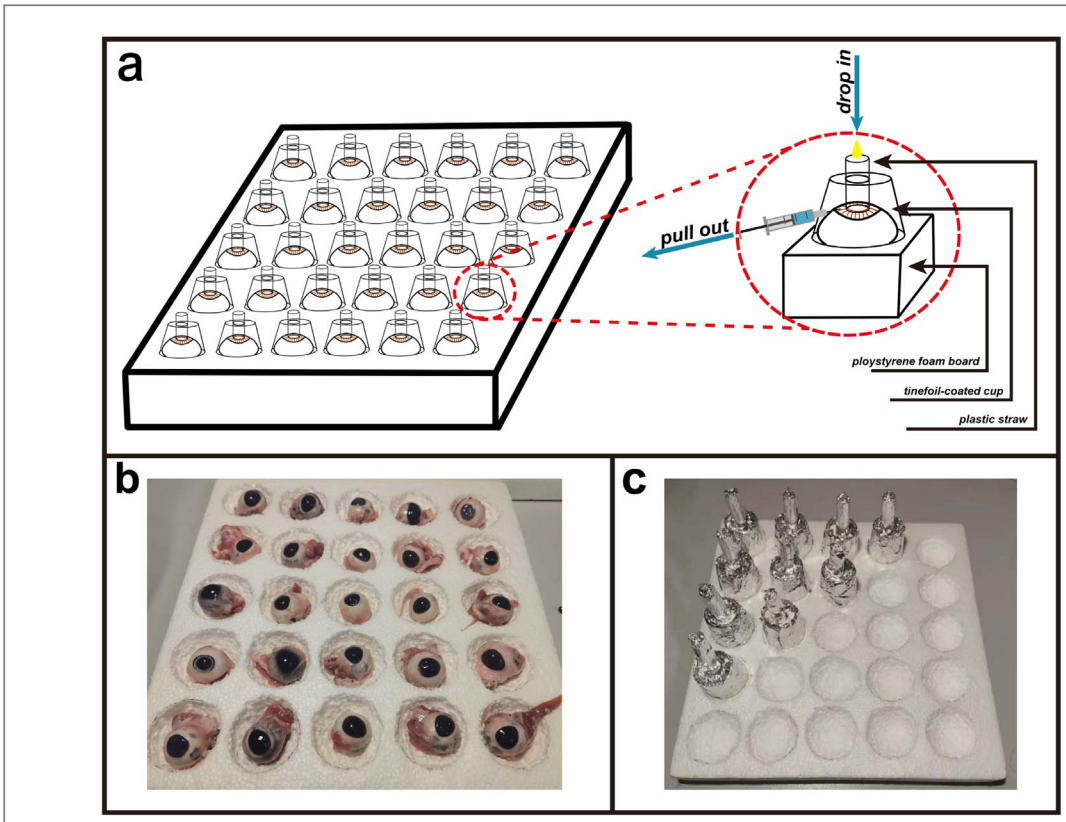

Figure 1. (A) special experimental setup based on Franz-type diffusion cells. (a) Schematic diagram of the Experimental setup. (b) Photograph of the experimental setup fully loaded with pig eyeballs. (c) Photograph of the complete experimental setup.

within a polystyrene foam board, and the corneal surfaces were gently cleaned with a PBS-soaked swab. To ensure stability, excess muscle tissue around the porcine eyes was carefully trimmed.

Nanocarrier solutions (15 mg mL^{-1}) were diluted 50 times with PBS to create a 0.3 mg mL^{-1} diluent, and 30 μl of this diluent was precisely administered onto the corneal surface using a pipettor. The contact area between the diluent and the cornea was 0.234 cm^2. To ensure uniform distribution of nanocarriers within the aqueous humor, the eyes were gently shaken 10 times before the aqueous humor was extracted at one-hour intervals. The total experimental duration was 6 h, with the temperature maintained at a constant 37 °C to simulate physiological conditions.

The extracted aqueous humor was filtered through a 0.22 μm nylon filter, and 50 μl of the filtered sample was added to each well of a microplate. Fluorescence intensity of FITC was measured using a microplate reader with excitation and emission wavelengths of 488 nm and 525 nm, respectively. The time-fluorescence intensity curves were generated based on measurement from three groups, with six sampling points per eye, five eyes per group, and three types of nanocarriers, resulting in the use of 90 eyes in total.

2.2.2. Standard curve

The aqueous humor was removed from 15 porcine eyes with a 1 mL syringe, and the syringe was inserted into a 0.22 μm needle filter and the aqueous humor was transferred to a container for later use. Filtered clear aqueous humor was used to dilute the nanocarrier solution (15 mg mL^{-1}) to create a series of six dilutions: 0.0125, 0.025, 0.0375, 0.05, 0.0625, and 0.075 mg mL^{-1}. Subsequently, pipette 50 μl of each set of dilutions accurately into the well of a black 96-well plate. Then, put the black 96-well plate into the microplate reader to measure the fluorescence intensity of the sample. The excitation and emission wavelengths of the microplate reader were 488 nm and 525 nm, respectively. The standard curve was obtained by linear fitting of the relationship between fluorescence intensity and concentration using the analysis module in Origin 2024 (OriginLab Corporation, Northampton, Massachusetts, USA).

2.2.3. Theory model

The permeation of nanocarriers into the cornea can be approximately modeled as a diffusion process driven by the concentration gradient. To describe this diffusion precession by math, some hypotheses are needed [33].

a) The concentration of the nanocarrier on the cornea surface is homogeneous and constant, ignoring the effects of gravity, temperature, and other external factors;

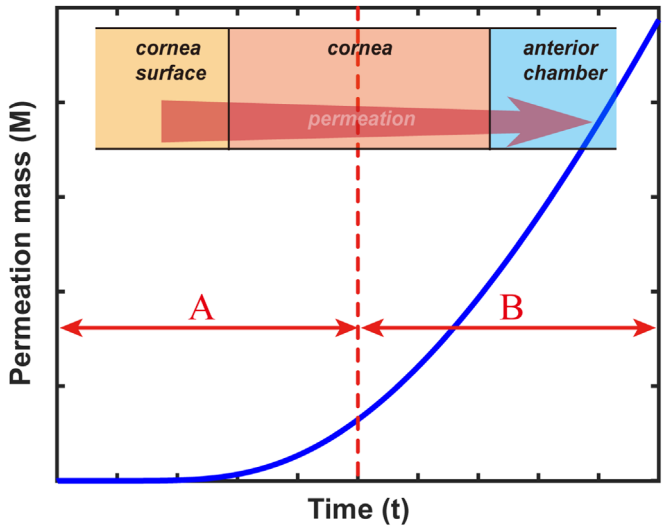

Figure 2. The ideal quality of nanocarrier accumulation across unit area cornea.

b) In the beginning, the concentration of nanocarrier within the cornea and aqueous humor is zero;

c) The diffusion coefficient of the nanocarrier within the cornea is uniform and constant;

d) The nanocarrier does not stay at the interface between the cornea and the anterior chamber, in other words, the concentration of the nanocarrier on that interface is zero;

e) The whole diffusion process can be approximated as a one-dimensional physical process.

According to Fick's law of diffusion, diffusion of nanocarriers within the cornea could be described by the following partial differential equation:

$$\frac{\partial C}{\partial t} = D\frac{\partial^2 C}{\partial x^2}(0 \leqslant x \leqslant l) \tag{1}$$

where C indicates the concentration of the nanocarrier on the location x at time t, t is permeation time, x represents any position within the cornea along the direction of thickness, and l denotes the corneal thickness, and D refers to the diffusion coefficient. The initial equation is as follows:

$$t = 0,\ C(x,\ t) = 0 \tag{2}$$

The boundary equations are as follows:

$$x = 0, \quad t > 0,\ C(x,\ t) = C_0 \tag{3}$$

$$x = l,\ t > 0,\ C(x,\ t) = 0 \tag{4}$$

where C_0 expresses the concentration of nanocarriers on the corneal outer surface at time zero. Based on the above equations, the solution of distribution of concentration of nanocarrier within the cornea is that:

$$C(x,\ t) = C_0\left(1 - \frac{x}{l}\right) - \frac{2C_0}{\pi}\sum_{n=1}^{\infty}\frac{1}{n} \times \sin\frac{n\pi x}{l}\exp\left(-\frac{n^2\pi^2}{l^2}Dt\right) \tag{5}$$

Taking Fick's first law ($J = -D\frac{\partial C}{\partial x}$) together with equation (5) could get an expression for diffusion flux (or J) at the interface between the cornea and the anterior chamber.

$$J(t)\ |_{x=l} = \frac{C_0 D}{l}\left[1 + 2\sum_{n=1}^{\infty}(-1)^n \exp\left(-\frac{n^2\pi^2}{l^2}Dt\right)\right] \tag{6}$$

Integrating the diffusion flux over time:

$$M(t) = \int_0^t J(\tau)d\tau \tag{7}$$

Taking equation (6) together with equation (7), the amount of nanocarrier accumulation (M) through the endothelial surface per unit area of the cornea can be expressed as follows:

$$M(t)|_{x=l} = C_0 l\left[\frac{Dt}{l^2} - \frac{2}{\pi^2}\sum_{n=1}^{\infty}\frac{(-1)^n}{n^2} \times \exp\left(-\frac{n^2\pi^2}{l^2}Dt\right) - \frac{1}{6}\right] \tag{8}$$

So, the ideal change of unit area transcorneal diffusion with time is shown in figure 2. The drug accumulation rate is slow in stage A, and the reason is that the drug is not yet totally across through the cornea. That rate is approximately consistent in stage B, as the distribution of drug concentration in the cornea tends to balance.

2.2.4. Statistical analysis

Statistical analysis of the results was performed using one-way analysis of variance (ANOVA). The statistical

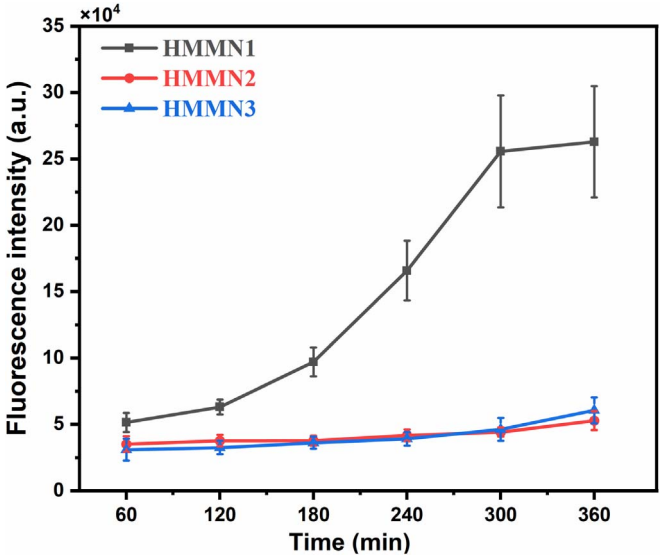

Figure 3. Fluorescence intensity analysis of FITC-labeled HMMN1-3 in aqueous humor within 360 min (mean ± SD, n = 5/group) (HMMN1-3 denote nanocarrier modified with thioether, biphenyl, and thioether/phenylene, respectively.).

analysis was computed with the SPSS 21.0 (IBM, Chicago, IL). Differences were considered significant when $p < 0.05$.

3. Result and discussion

3.1. Comparison of penetration capacity of nanocarriers

The permeation capacity of the nanocarriers was assessed by the fluorescence intensity in the aqueous humor, which correlates with the amount of FITC-labeled nanocarriers permeating through the cornea. Over a period of 360 min, the fluorescence intensity was recorded hourly using a microplate reader.

The fluorescence intensity of HMMN1 was significantly higher compared to both HMMN2 and HMMN3 ($p < 0.05$), while no significant difference was observed between HMMN2 and HMMN3 in their transcorneal permeation capacity. Figure 3 illustrates the fluorescence intensity of FITC-labeled HMMN1, HMMN2, and HMMN3 in the aqueous humor over 6 h (mean ± SD, n = 5 per group). The results indicate a significant difference in fluorescence intensity between HMMN1 and both HMMN2 and HMMN3 ($p < 0.05$). However, no significant difference was observed between HMMN2 and HMMN3 in their ability to penetrate through the cornea. The significantly higher fluorescence intensity observed in the aqueous humor containing HMMN1 compared to the other nanocarriers suggests that the thioether moieties in HMMN1 enhance transcorneal permeation more effectively than the biphenyl moieties in HMMN2 or the thioether/phenylene combination in HMMN3.

This enhanced permeability suggests that while thioether facilitates the transcorneal permeation process, biphenyl may have a less pronounced effect, and the presence of phenylene in the thioether/phenylene combination could even negatively impact transcorneal permeability. These findings are consistent with our previous results [21], which reported that thioether-hybridized HMMN exhibited the strongest corneal penetration capacity.

Given the superior corneal permeability of HMMN1, further analysis through a standard curve experiment was conducted to establish the relationship between its permeation quality and time.

3.2. Standard curve study

To calculate the diffusion coefficient, determining the temporal variation of HMMN1 corneal penetration mass per unit area is required. The temporal variation was achieved through a three-step analytical process: First, a calibration curve was established by measuring the fluorescence intensity of aqueous humor samples containing known concentrations of the nanocarrier. Subsequently, the experimentally observed fluorescence intensities were correlated with corresponding nanocarrier concentrations using a linear regression model implemented in the fitting module of Origin 2024 software. Then, the time-dependent fluorescence intensity of the aqueous humor containing the nanocarrier was converted to the corresponding mass of the nanocarrier using the linear relationship established earlier. The relationship between fluorescence intensity and mass of HMMN1 is presented in figure 4.

It's important to note that the fluorescence intensity depicted in figure 3 represents the emission from the nanocarrier contained in 50 μl of aqueous humor. Given that the volume of aqueous humor in porcine eyes is comparable to that in human eyes, approximately 300 μl [34, 35], the total mass of the nanocarrier in the porcine eye was calculated to be six times the amount present in each well of the microplate.

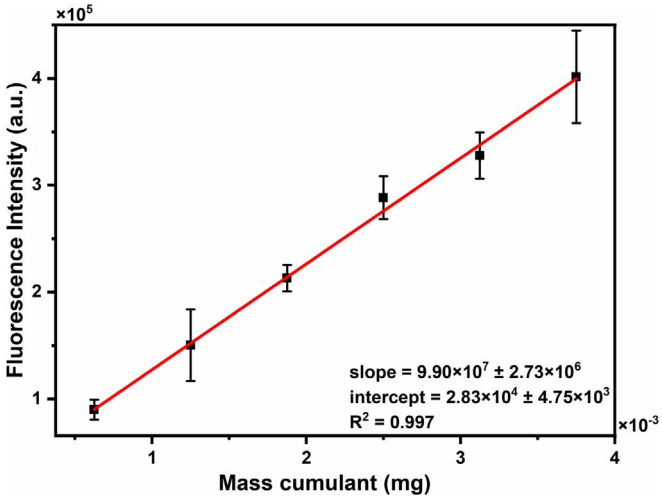

Figure 4. Fitting regression equation diagram about fluorescence intensity and mass of HMMN1 (mean ± SD, n = 5).

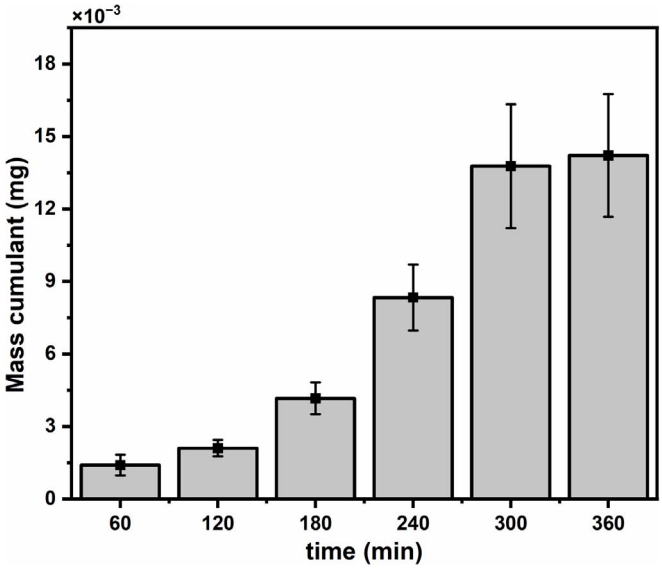

Figure 5. Mass accumulation of HMMN1 in aqueous humor of one porcine eye within 360 min (mean ± SD, n = 5).

Therefore, the mass of nanocarriers carried by the aqueous humor sample (50 μl) collected from the micropores at each sampling time point was multiplied by 6 to represent the cumulative amount of nanocarriers in the aqueous humor up to that sampling time.

Figure 5 illustrates the mass accumulation of nanocarrier in the aqueous humor of a porcine eye over 360 min, demonstrating a consistent upward trend. Note that the one porcine eye here is the average of the aqueous humor taken at each sampling point (containing 5 eyes). The most pronounced increase in mass occurred within the first 300 min, with the growth rate per hour notably accelerating between 120 and 240 min. Subsequently, the growth rate began to decline, showing a significant decrease during the 300–360 min interval.

This behavior can be interpreted as follows: in the initial phase, HMMN1 had not fully penetrated the cornea, resulting in a low concentration in the aqueous humor and a slower rate of mass increase. In the intermediate phase, once HMMN1 successfully permeated the cornea and established a stable concentration gradient, the content in the aqueous humor increased at a relatively constant rate. In the final phase, the cumulative mass rate of HMMN1 in the aqueous humor slowed and neared zero, likely due to the stabilization of HMMN1 distribution within the cornea. As the concentration of nanocarrier at the posterior corneal surface closes that in the aqueous humor, the resulting diminished concentration gradient becomes insufficient to drive further nanocarrier permeation through the cornea. The observed trend in the mass accumulation of HMMN1 is consistent with

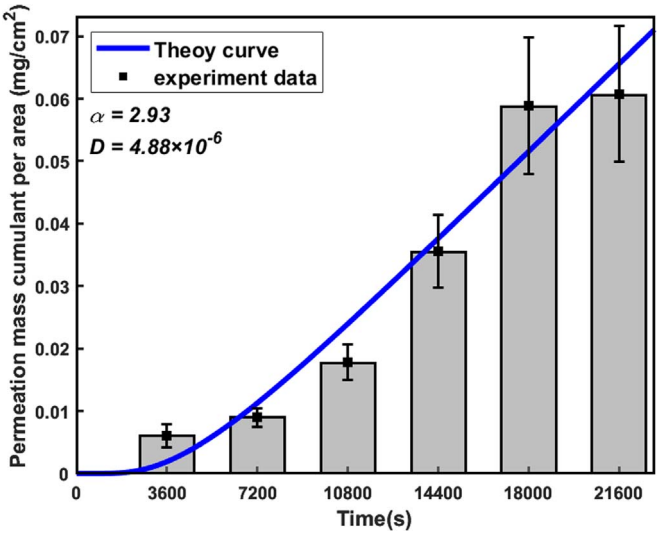

Figure 6. The mass permeation of HMMN1 through per unit area of the cornea over time (α presents the corneal thickness correction factor, D is the cornea diffusion coefficient of HMMN1).

the cumulative permeation curve of riboflavin in bovine corneas, as reported by Morrison *et al* [36]. Additionally, this trend aligns with findings from Gómez-Segura *et al* who studied the cumulative permeation of carprofen in porcine corneas [37], and Rasoanirina *et al* who examined the permeation of a self-nanoemulsifying drug delivery system and VFEND® IV in bovine corneas [38]. The absence of a third phase in their cumulative permeation curves, however, may be attributed to shorter experimental durations compared to the current study. In addition, some emerging techniques that enhance drug penetration through corneal epithelium—such as femtosecond laser-assisted micro-holes [39] and low-current iontophoresis [40]—may further improve the corneal permeability of nanocarriers.

3.3. Corneal permeability parameters of HMMN1

The mathematical model can effectively capture certain aspects of the actual diffusion process of the nanocarrier within the cornea. However, due to differences between the mathematical model and the actual situation, a corneal thickness correction factor, α, was introduced to better describe the real process. The corneal thickness is 0.125 cm [41]. Therefore, the corrected corneal thickness $l' = \alpha \cdot l$. The mathematical model was fitted to the experimental data to obtain α and D. As shown in figure 6, the model fits the data better during the steady phase of the mass accumulation rate.

The corrected model parameters obtained from regression analysis of the experimental data are $\alpha = 2.93$ and $D = 4.88 \times 10^{-6}$ cm^2/s. Meanwhile, considering that the apparent permeability coefficient (Papp) is widely used in the field of drug development, it can be used to evaluate the ability of drugs to penetrate biomembranes and predict the bioavailability and efficacy of drugs. Papp was calculated from figure 6 using the following equation:

$$P_{app} = \frac{\Delta M}{\Delta t \cdot C_0 \cdot A} \tag{9}$$

where $\Delta M/\Delta t$ is the slope of the linear portion of the plot between the mass of the nanocarrier in the aqueous humor and time, A is the area of the cornea exposed to the diluent, and C_0 is the initial concentration of the diluent.

Based on the slope of the curve during the stable phase of the mass change rate in figure 6, which is 3.90×10^{-6}, the Papp of HMMN1 across the cornea was calculated to be 1.30×10^{-5} cm s^{-1}.

The model's fit to the experimental values was relatively poor in the initial stages due to the omission of gravity's effect, which could have had a minor positive influence on the nanocarrier permeation through the cornea. Additionally, the model assumes that the nanocarrier at the posterior corneal surface is indefinitely diluted by the aqueous humor. However, since the volume of the aqueous humor isn't infinite, the concentration of nanocarriers in the aqueous humor will eventually align with that at the posterior corneal surface. As a result, the predictions of the model deviate significantly from the experimental data in the later stages.

As a mesoporous silica nanoparticle, the Papp of HMMN1 in porcine corneas (1.30×10^{-5} cm s^{-1}) is higher than that of Aminated Mesoporous Silica Nanoparticles loaded with 5-Fluorouracil (AMSN-FU) and Aminated Mesoporous Silica Nanoparticles coated with Carboxymethyl Chitosan and loaded with 5-Fluorouracil (AMSN-CMC-FU) in goat corneas (2.17×10^{-6} cm^2 s^{-1}, 3.42×10^{-6} cm s^{-1}) [42]. Therefore, HMMN1 has great corneal permeability.

Although the porcine eye is an ideal model for ocular drug experiments due to its similarity in

physical size, histology, physiology, and endothelial thickness to human eyes [43, 44], there are important differences to consider. The corneal epithelium in the porcine eye is approximately twice as thick as humans, and the corneal stroma is about 30% thicker [31]. Consequently, the diffusion coefficient obtained in this study may be slightly lower than what would be expected in human corneal administration [45]. Despite these differences, our findings provide valuable data that can support experimental and numerical studies related to the transport of nanoparticle-based drug delivery [46].

4. Conclusions

This study investigated the transcorneal permeability of nanocarriers modified with three distinct organic moieties: thioether, biphenyl, and thioether/phenylene. The corneal penetration experiments provided time-dependent data on the content of each nanocarrier in the aqueous humor.

The findings demonstrate that thioether significantly enhances transcorneal permeation, achieving a corneal diffusion coefficient of 4.88×10^{-6} cm^2 s^{-1} and an apparent permeability coefficient (Papp) of 1.30×10^{-5} cm s^{-1}. In contrast, biphenyl modifications exhibit limited efficacy, while the thioether/phenylene modification shows poor transcorneal permeability, suggesting that phenylene potentially impedes permeation.

These results not only advance understanding of the corneal permeation process of nanocarriers and the significant role played by organic groups in this process, but also provide valuable data references for future experimental and numerical simulation studies on nanocarriers.

Acknowledgments

This project was financially supported by the National Science Foundation China (nos. 82070959, nos. 82271082), the General project of Shanghai Natural Science Foundation (nos. 21ZR1411500, nos. 22ZR1409900), the Medical Engineering Joint Fund of Fudan University (nos. YG202213). We thank the School of Health Science and Engineering of University of Shanghai for Science and Technology for providing equipment support.

Data availability statement

All data that support the findings of this study are included within the article (and any supplementary files).

Ethical statement

All experiments complied with the Association for Research in Vision and Ophthalmology Statement on the use of animals in ophthalmic and vision research. The animal study was approved by the Animal Care and Use Committee of Eye and ENT Hospital of Fudan University (Shanghai, China).

ORCID iDs

Yonghui Qiao https://orcid.org/0000-0001-9275-8887

References

[1] Jayaram H, Kolko M, Friedman D S and Gazzard G 2023 Glaucoma: now and beyond *Lancet* **402** 1788–801
[2] Xu Y, Tan Q, Li C and Liu D 2022 The ocular biometry characteristics of young patients with primary angle-closure glaucoma *BMC Ophthalmol* **22** 150
[3] Kumar H and Taneja S 2025 Double-frequency Nd:YAG laser reduction of peripheral iridotomy size for treatment of visual symptoms *Indian Journal of Ophthalmology* **73** S341
[4] Luo S, Mikula E R, Khazaeinezhad R, Bradford S M, Zhang F, Jester J V and Juhasz T 2024 Evaluating the effect of pulse energy on femtosecond laser trabeculotomy (FLT) outflow channels for glaucoma treatment in human cadaver eyes *Lasers in Surgery and Medicine* **56** 382–91
[5] Zgryźniak A, Przeździecka-Dołyk J, Szaliński M and Turno-Kręcicka A 2021 Selective laser trabeculoplasty in the treatment of ocular hypertension and open-angle glaucoma: clinical review *Journal of Clinical Medicine* **10** 3307
[6] Patton G N and Lee H J 2024 Chemical insights into topical agents in intraocular pressure management: from glaucoma etiopathology to therapeutic approaches *Pharmaceutics* **16** 274
[7] Akulo K A, Adali T, Moyo M T G and Bodamyali T 2022 Intravitreal Injectable hydrogels for sustained drug delivery in glaucoma treatment and therapy *Polymers* **14** 2359
[8] Wang Y and Wang C 2022 Novel eye drop delivery systems: advance on formulation design strategies targeting anterior and posterior segments of the eye *Pharmaceutics* **14** 1150
[9] Cvenkel B and Kolko M 2022 Devices and treatments to address low adherence in glaucoma patients: a narrative review *JCM* **12** 151
[10] Londhe V Y and Sharma S 2022 Formulation, characterization, optimization and *in-vivo* evaluation of methazolamide liposomal *in situ* gel for treating glaucoma *J. Drug Delivery Sci. Technol.* **67** 102951
[11] Zhang F, Chen H, Lan J, Song K and Wu X 2021 Preparation and *in vitro/in vivo* evaluations of novel ocular micelle formulations of hesperetin with glycyrrhizin as a nanocarrier *Experimental Eye Research* **202** 108313
[12] Albarqi H A, Garg A, Ahmad M Z, Alqahtani A A, Walbi I A and Ahmad J 2023 Recent Progress in Chitosan-Based Nanomedicine for Its Ocular Application in Glaucoma *Pharmaceutics* **15** 681
[13] Lancina M G, Singh S, Kompella U B, Husain S and Yang H 2017 Fast dissolving dendrimer nanofiber mats as alternative to eye drops for more efficient antiglaucoma drug delivery *ACS Biomater. Sci. Eng.* **3** 1861–8
[14] Radwan S E-S, El-Moslemany R M, Mehanna R A, Thabet E H, Abdelfattah E-Z A and El-Kamel A 2022 Chitosan-coated bovine serum albumin nanoparticles for topical tetrandrine delivery in glaucoma: *in vitro* and *in vivo* assessment *Drug Deliv.* **29** 1150–63
[15] Rubenicia A M L, Cubillan L D P, Sicam V A D P, Macabeo A P G, Villaflores O B and Castillo A L 2021 Intraocular pressure reduction effect of 0.005% latanoprost

eye drops in a hyaluronic acid-chitosan nanoparticle drug delivery system in albino rabbits *Trans. Vis. Sci. Tech.* **10** 2
[16] Amankwa C E, Gondi S R, Dibas A, Weston C, Funk A, Nguyen T, Nguyen K T, Ellis D Z and Acharya S 2021 Novel thiol containing hybrid antioxidant-nitric oxide donor small molecules for treatment of glaucoma *Antioxidants* **10** 575
[17] Cavet M E, Vittitow J L, Impagnatiello F, Ongini E and Bastia E 2014 Nitric oxide (NO): an emerging target for the treatment of glaucoma *Invest. Ophthalmol. Vis. Sci.* **55** 5005
[18] Aliancy J, Stamer W D and Wirostko B 2017 A review of nitric oxide for the treatment of glaucomatous disease *Ophthalmol Ther* **6** 221–32
[19] Reina-Torres E, De Ieso M L, Pasquale L R, Madekurozwa M, Van Batenburg-Sherwood J, Overby D R and Stamer W D 2021 The vital role for nitric oxide in intraocular pressure homeostasis *Progress in Retinal and Eye Research* **83** 100922
[20] Lei Y, Gao Y, Song M, Cao W and Sun X 2020 Peroxynitrite is a novel risk factor and treatment target of glaucoma *Nitric Oxide* **99** 17–24
[21] Song M *et al* 2023 Peroxynitrite-scavenging organosilica nanomedicines for light-controllable NO release and precision on-demand glaucoma therapy *ACS Nano* **17** 20979–90
[22] Gao F *et al* 2019 Biodegradable, pH-sensitive hollow mesoporous organosilica nanoparticle (HMON) with controlled release of pirfenidone and ultrasound-target-microbubble-destruction (UTMD) for pancreatic cancer treatment *Theranostics* **9** 6002–18
[23] Huang P, Chen Y, Lin H, Yu L, Zhang L, Wang L, Zhu Y and Shi J 2017 Molecularly organic/inorganic hybrid hollow mesoporous organosilica nanocapsules with tumor-specific biodegradability and enhanced chemotherapeutic functionality *Biomaterials* **125** 23–37
[24] Chen J *et al* 2022 Hollow mesoporous organosilica nanotheranostics incorporating formimidoyltransferase cyclodeaminase (FTCD) plasmids for magnetic resonance imaging and tetrahydrofolate metabolism fission on hepatocellular carcinoma *Int. J. Pharm.* **612** 121281
[25] Zhang C *et al* 2023 Hollow mesoporous organosilica nanoparticles reduced graphene oxide based nanosystem for multimodal image-guided photothermal/photodynamic/chemo combinational therapy triggered by near-infrared *Cell Proliferation* **56** e13443
[26] Fan W, Song M, Li L, Niu L, Chen Y, Han B, Sun X, Yang Z, Lei Y and Chen X 2021 Endogenous dual stimuli-activated NO generation in the conventional outflow pathway for precision glaucoma therapy *Biomaterials* **277** 121074
[27] Li J *et al* 2024 Evaluation of the ocular safety of hollow mesoporous organosilica nanoparticles with different tetrasulfur bond content *IJN* **19** 7123–36
[28] Natesan S, Pandian S, Ponnusamy C, Palanichamy R, Muthusamy S and Kandasamy R 2017 Co-encapsulated resveratrol and quercetin in chitosan and peg modified chitosan nanoparticles: for efficient intra ocular pressure reduction *Int. J. Biol. Macromol.* **104** 1837–45
[29] Huang J, Peng T, Li Y, Zhan Z, Zeng Y, Huang Y, Pan X, Wu C-Y and Wu C 2017 Ocular cubosome drug delivery system for timolol maleate: preparation, characterization, cytotoxicity, *ex vivo*, and *in vivo* evaluation *AAPS Pharm. Sci. Tech.* **18** 2919–26
[30] Wang F, Bao X, Fang A, Li H, Zhou Y, Liu Y, Jiang C, Wu J and Song X 2018 Nanoliposome-encapsulated brinzolamide-hydropropyl-β-cyclodextrin inclusion complex: a potential therapeutic ocular drug-delivery system *Front. Pharmacol.* **9** 91
[31] De Hoon I, Boukherroub R, De Smedt S C, Szunerits S and Sauvage F 2023 *In vitro* and *ex vivo* models for assessing drug permeation across the cornea *Mol. Pharmaceutics* **20** 3298–319
[32] Cardoso T P de A, Kishishita J, Souza A T M, Vieira J R C, Melo C M L de, Santana D P de and Leal L B 2020 A proposed eye *ex vivo* permeation approach to evaluate pesticides: case dimethoate *Toxicol. in Vitro* **66** 104833
[33] Ouriemchi E M and Vergnaud J M 2000 Processes of drug transfer with three different polymeric systems with transdermal drug delivery *Comput. Theor. Polym. Sci.* **10** 391–401
[34] Alshaikh R A, Waeber C and Ryan K B 2022 Polymer based sustained drug delivery to the ocular posterior segment: barriers and future opportunities for the treatment of neovascular pathologies *Adv. Drug Delivery Rev.* **187** 114342
[35] Shrader S M and Greentree W F 2018 Göttingen minipigs in ocular research *Toxicol Pathol* **46** 403–7
[36] Morrison P W J and Khutoryanskiy V V 2014 Enhancement in corneal permeability of riboflavin using calcium sequestering compounds *Int. J. Pharm.* **472** 56–64
[37] Gómez-Segura L, Parra A, Calpena A C, Gimeno Á and Boix-Montañes A 2020 Carprofen permeation test through porcine *ex vivo* mucous membranes and ophthalmic tissues for tolerability assessments: validation and histological study *Veterinary Sciences* **7** 152
[38] Rasoanirina B N V, Lassoued M A, Kamoun A, Bahloul B, Miladi K and Sfar S 2020 Voriconazole-loaded self-nanoemulsifying drug delivery system (SNEDDS) to improve transcorneal permeability *Pharm. Dev. Technol.* **25** 694–703
[39] Bradford S, Joshi R, Luo S, Farrah E, Xie Y, Brown D J, Juhasz T and Jester J V 2024 *In vivo* femtosecond laser machined transepithelial nonlinear optical corneal crosslinking compared to ultraviolet corneal crosslinking *Translational Vision Science & Technology* **13** 9
[40] Joshi R, Bradford S, Luo S, Farrah E, Xie Y, Brown D J, Juhasz T and Jester J V 2025 Enhanced riboflavin stromal delivery using microchannel-assisted iontophoresis for corneal crosslinking *Translational Vision Science & Technology* **14** 18
[41] Menduni F, Davies L N, Madrid-Costa D, Fratini A and Wolffsohn J S 2018 Characterisation of the porcine eyeball as an *in-vitro* model for dry eye *Contact Lens and Anterior Eye* **41** 13–7
[42] Alhowyan A A, Kalam M A, Iqbal M, Raish M, El-Toni A M, Alkholief M, Almomen A A and Alshamsan A 2023 Mesoporous silica nanoparticles coated with carboxymethyl chitosan for 5-fluorouracil ocular delivery: characterization, *in vitro* and *in vivo* studies *Molecules* **28** 1260
[43] Alambiaga-Caravaca A M, Calatayud-Pascual M A, Rodilla V, Concheiro A, López-Castellano A and Alvarez-Lorenzo C 2020 Micelles of progesterone for topical eye administration: interspecies and intertissues differences in *ex vivo* ocular permeability *Pharmaceutics* **12** 702
[44] Pescina S, Govoni P, Potenza A, Padula C, Santi P and Nicoli S 2015 Development of a convenient *ex vivo* model for the study of the transcorneal permeation of drugs: histological and permeability evaluation *J. Pharm. Sci.* **104** 63–71
[45] Reichl S, Bednarz J and Müller-Goymann C C 2004 Human corneal equivalent as cell culture model for *in vitro* drug permeation studies *Br. J. Ophthalmol.* **88** 560–5
[46] Qiao Y, Wang Y, Chen Y, Luo K and Fan J 2022 Mathematical modeling of shear-activated targeted nanoparticle drug delivery for the treatment of aortic diseases *Biomech. Model. Mechanobiol.* **21** 221–30